A Voyage to Africa by Mr Swift

Niklas Wahlström and Fredrik Gustafsson
Department of Electrical Engineering
Linköping University
Email: {nikwa, fredrik}@isy.liu.se

Susanne Åkesson
Department of Ecology
Lund University
Email: susanne.akesson@biol.lu.se

***Abstract*—A male common swift *Apus apus* was equipped with a light logger on August 5, 2010, and again captured in his nest 298 days later. The data stored in the light logger enables analysis of the fascinating travel it made in this time period.**

The state of the art algorithm for geolocation based on light loggers consists in computing first sunrise and sunset from the logged data, which are then converted to midday (gives longitude) and day length (gives latitude). This approach has singularities at the spring and fall equinoxes, and gives a bias for fast day transitions in the east-west direction.

We derive a flexible particle filter solution, where sunset and sunrise are processed in separatele measurement updates, and where the motion model has two modes, one for migration and one for stationary long time visits, which are designed to fit the flying pattern of the swift. This approach circumvents the aforementioned problems with singularity and bias, and provides realistic confidence bounds on the geolocation as well as an estimate of the migration mode.

***Index Terms*—nonlinear filtering, particle filter, geolocation, light levels**

Fig. 1: A male common swift after his voyage to Africa and back. During the journey a light logger mounted to his back recording the light intensity.

I. Introduction

Geolocation for learning migration behavior of animals is an important area for ecologists and epidemiologists. With an ever lasting improvement in sensor technology and miniturization of electronics, more and smaller species can be studied. More specifically, researchers are no longer limited to satellite based geolocation, which requires substantial battery capacity and in practice also radio transmitters to communicate the geolocation data, which in turn requires even more battery with the consequence that only larger birds can be studied. One such enabling technology is light loggers permitting documentation of migration by individual small songbirds, waders and swifts, which so far is not extensively studied. Commercial versions include a light sensor, a battery, a memory and a clock enclosed in a small housing that can be fit to the tarsus or mounted with a harness to the back of the bird. As a rule of thumb, the sensor can weigh at most 5% of a bird's weight. State of the art sensors weigh 2 grams, and thus as small birds as a swift (40g) can be marked. The sensor unit cannot communicate, so this approach hinges on that the birds are caught or found when they die, so the memory can be read off.

The swift is an interesting bird, since it is believed to spend all of its life on the wings, except for the nesting period. This makes the light data particular good, since there is barely any surrounding vegetation that disturb the measurements. Also the migration pattern of the swift is fascinating, since it travels long distances over the seasons, but always returns to basically the same place for mating in the summer. This unique navigation ability is believed to be genetically inherited, and it might have persisted since the last ice age. The swift in Figure 1 is a young male and one of the first marked swift that has been found. The researchers know very little about the migration pattern for swifts during the winter time in Africa, since there are almost no reports from Africa on found species with the classical ring.

The light logger samples light intensity every 5-10 minutes. It is quite a course information suffering from saturation at both ends. Thus, it is only the transitions between night and day and *vice versa* that contain information with the current sensor. The theory of geolocation by light levels is described in [1] for elephant seals, where sensitivity and geometrical relations are discussed in detail. The accuracy of the geolocation is evaluated on different sharks by comparing to a satellite navigation system, and the result is shown to be in the order of 1 degree in longitude and latitude.

If the animal is known to be at rest during the night, the two positions corresponding to sunset and sunrise can be assumed the same, and the unknown longitude and latitude can be solved from the two measurements uniquely. This is the basis for the geolocation software that comes with the sensor. There is an obvious singularity for the two days of

equinox when the sun is in the same plane as the equator, and thus the two manifolds in Figure 2 are vertical lines. In praxis 15 days on each side of spring and autumn equinoxes are omitted from analyses [2]. Another problem occurs if the bird is moving between sunrise and sunset, in which case midday and daylength is shifted slightly causing a bias in the position. This is especially a problem during fast migration flights, when a swift may cover up to 650 km/day [3].

Fig. 2: Binary day-light model for a particular time t. The shape of the dark area depends on the time of the year, and the horizontal position of the dark area depends on the time of the day.

We propose a nonlinear filtering framework, where the sunset and sunrise are treated as separate measurement updates, and an irregularly sampled motion model is used for the time update. This removes the bias problem and also a noise correlation artifact. It also mitigates the singularity at the equinox, where still useful positions can be computed. The motion model has two modes, corresponding to stationary and migrating flight. The filter thus has adaptive sensitivity, giving higher position accuracy at the stationary mode.

Animal geolocation based on light levels can be traced back to at least l986 [4]. Other publications such as [5], [1], [6] and [2] have also studied this problem. However, to the best of the authors knowledge, this is the first time that this applications has been put into a statistical filtering framework.

The paper outline is as follows: In Section II an appropriate sensor and motion model for this application will be presented and the state estimation algorithm is given in Section III. The paper is concluded with the results on real world data in Section IV followed by the conclusions in Section V.

II. Models

The mathematical framework can be summarized in a state space model with state x_k, position dependent measurement y_k, process noise w_k, and measurement noise e_k:

$$x_{k+1} = f(x_k, w_k), \tag{1a}$$

$$y_k = h(x_k) + e_k. \tag{1b}$$

The state includes position (X_k, Y_k) encoded as longitude X_k and latitude Y_k, a velocity $(\dot{X}_k, \dot{Y}_k)$ as well as a mode parameter δ_k with two modes, one for migration and one for stationary long time visits.

A. Sunrise and Sunset Models

Figure 2 shows how the sunset and sunrise, respectively, at each time defines a manifold on earth [7]. A sensor consisting of a light-logger and clock can detect these two events. The bright part of the earth is limited by a great circle orthogonal to the sun at each time.

The time of the sunrise and sunset can easily be derived when knowing the daylength and the time of the midday. The midday will only depend on the longitude of the observer. At longitude $X_k = 0°$ the midday occurs at 12.00 noon. When going $X = 360°/24 = 15°$ east, the midday occurs one hour earlier at 11.00 a.m (earlier, since the sun rises in the east). This gives the relation

$$h^{\text{midday}}(X_k) = 12 - \frac{1}{15} X_k. \tag{2}$$

Further, the daylength will depend on the latitude of the observer as well as on the time of the year. The relation can be derived by making use of the coordinate transformation from the equatorial coordinate system to the horizontal coordinate system. These coordinate systems are used for mapping positions on the celestial sphere and can thus be used for describing the position of the sun.

The horizontal coordinate system uses the observer's local horizon as the fundamental plane and the position of the sun is described with its altitude h above the horizon and its azimuth A measured from the south increasing towards the east, see Figure 3.

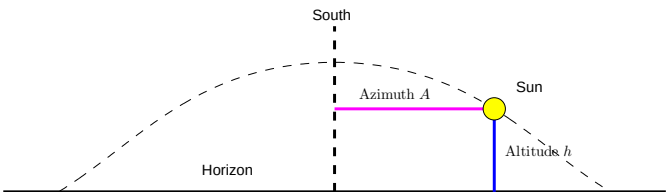

Fig. 3: The horizontal coordinate system.

In the equatorial coordinate system the fundamental plane is defined by the Earth's equator. Here the position of the sun is described with the solar hour angle H expressed in angular measurement from the solar noon, and the declination of the sun δ.

All of these four angles are defined on the celestial sphere [7], [8]. However, in this work we are interested in describing the position of the observer on the earth rather than the position of the sun on the celestial sphere. Therefore, in Figure 4, the corresponding angles on the earth are depicted. Here, the altitude h has the interpretation of being the orthogonal distance (measured in degrees) to the great circle separating the bright and dark part of the earth, the hour angle H will be the longitude relative to the solar noon meridian and the declination δ is the tilt of the earth's axis towards the sun as well as the latitude where the sun reaches its zenith.

These two coordinate systems are related as [7]

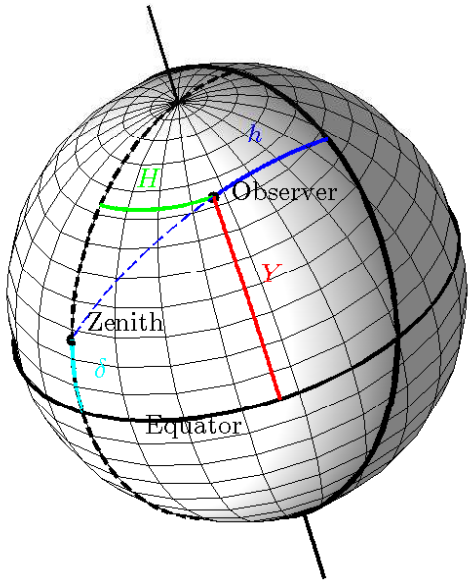

Fig. 4: The hour angle H, declination δ and altitude h projected on to the earth, together with the observer's latitude Y. The position "zenith" is the location where the sun is at its zenith. The geometry of these angles gives the relation (3a).

$$\sin h = \sin Y \sin \delta + \cos Y \cos \delta \cos H \tag{3a}$$

$$\tan A = \frac{\sin H}{\cos H \sin Y - \tan \delta \cos Y} \tag{3b}$$

where Y is the latitude of the observer. The declination of the sun can also be seen as the angle between the Earth's axis and a line perpendicular to the Earth's orbit. Thus, the declination will change over the year and is given by

$$\delta(t_k) = -23.439^\circ \cos\left(\frac{360^\circ}{365.25} t_k\right), \tag{4}$$

where t_k is the number of days after the winter solstice. Since a day of 24 hours corresponds to an hour angle of $H = 360^\circ$, (3a) gives us the relation

$$h^{\text{daylength}}(t_k, Y_k) = \frac{24}{360^\circ} \arccos\left(\frac{\sin h_0 - \sin Y_k \sin \delta(t_k)}{\cos Y_k \cos \delta(t_k)}\right) \tag{5}$$

The altitude h_0 is here considered as a constant. It represents the geometrical altitude of the sun at the time apparent rising and setting. Due to atmospheric refraction, these events occur already when the sun geometrically is below the horizon at an altitude of $h_0 = -0^\circ.83$ [7]. Furthermore, the light intensity starts increasing already before the sunrise and is still increasing after the event. Noticeable is that the most distinct transition between day and night occurs when the sun is about 6° below the horizon [1]. Thus, the altitude h_0 will in practice depend on how the light intensity data is thresholded.

Note that if the argument of arccosine in (5) is larger than 1 in absolute value, the sun will remain either above or below the horizon the whole day.

With this information we can define a measurement model for sunrise and sunset respectively

$$y^{\text{rise}}(t_k) = h^{\text{rise}}(t_k, X_k, Y_k) + e_k^{\text{rise}}, \tag{6a}$$

$$y^{\text{set}}(t_l) = h^{\text{set}}(t_l, X_l, Y_l) + e_l^{\text{set}}. \tag{6b}$$

where

$$h^{\text{rise}}(t_k, X_k, Y_k) = h^{\text{midday}}(X_k) - \frac{h^{\text{daylength}}(t_k, Y_k)}{2} \tag{6c}$$

$$h^{\text{set}}(t_l, X_l, Y_l) = h^{\text{midday}}(X_l) + \frac{h^{\text{daylength}}(t_l, Y_l)}{2} \tag{6d}$$

B. Sensor Error Model

The errors $e^{\text{rise}}(t_k)$ and $e^{\text{set}}(t_l)$ for sunrise and sunset, respectively, consist of different kinds of errors:

1) Detection errors from the light logger data. The data in Figure 7 indicates that this error is Gaussian with a standard deviation of slightly more than four minutes. Note that four minutes corresponds to 1 degree, which is 120 km in north-south direction and 120 times cosinus of latitude in east-west direction.
2) Position dependent variations. For instance, the days are longer over sea than land [1]. We will neglect this error, since the bird appears to be over land most of the time. It would be no problem to cover this in our framework, though.
3) Also the latitude and time of year may affect the error. This is a subject for future studies.
4) Weather dependent variations, where sunny days are longer than cloudy ones. This can be incorporated by using data from historic weather data bases in our framework, but this is also a subject for future studies.

Note that the errors in sunset and sunrise can be seen as independent, and thus the error in day length and midday are actually correlated.

C. Kinematic Model

The kinematic model of migrating birds is characterized by two modes consisting of a *stationary mode* on their breeding, wintering or moulting sites, as well as a *migration mode* [9]. The mode parameter $\delta_k \in \{$"stationary mode", "migration mode"$\}$ is here modeled as a hidden Markov state with a specified transition probability Π_k resulting in

$$p(\delta_{k+1}|\delta_k) = \Pi_k^{(\delta_{k+1}, \delta_k)} \tag{7}$$

In the stationary mode it is sufficient to model the bird with a *constant position* model. The states related to this model is only two dimensional position and is the simplest possible motion model

$$x(t) = \begin{pmatrix} X(t) \\ Y(t) \end{pmatrix}, \quad \dot{x}(t) = \begin{pmatrix} w^X(t) \\ w^Y(t) \end{pmatrix} \tag{8a}$$

The corresponding discrete time model is given by

$$x_{k+1} = \begin{pmatrix} 1 & 0 \\ 0 & 1 \end{pmatrix} x_k + \begin{pmatrix} T & 0 \\ 0 & T \end{pmatrix} \begin{pmatrix} w_k^X \\ w_k^Y \end{pmatrix}. \tag{8b}$$

In the migration mode the velocity of the bird will be of great importance when predicting the next position. This can be captured by using a *constant velocity* model. This is still a fairly simple motion model, yet one of the most common ones in target tracking applications where no inertial measurements are available. It is given by a two-dimensional version of Newton's force law:

$$x(t) = \begin{pmatrix} X(t) \\ Y(t) \\ \dot{X}(t) \\ \dot{Y}(t) \end{pmatrix}, \quad \dot{x}(t) = \begin{pmatrix} \dot{X}(t) \\ \dot{Y}(t) \\ w^X(t) \\ w^Y(t) \end{pmatrix} \tag{9a}$$

The corresponding discrete time model is given by

$$x_{k+1} = \begin{pmatrix} 1 & 0 & T & 0 \\ 0 & 1 & 0 & T \\ 0 & 0 & 1 & 0 \\ 0 & 0 & 0 & 1 \end{pmatrix} x_k + \begin{pmatrix} T^2/2 & 0 \\ T & 0 \\ 0 & T^2/2 \\ 0 & T \end{pmatrix} \begin{pmatrix} w_k^X \\ w_k^Y \end{pmatrix}. \tag{9b}$$

The process noise $w_k \sim \mathcal{N}(0, Q^{\delta_k})$ for the two modes is assumed to be white Gaussian. In order to capture the described kinematic of the bird we later choose process noise such that $TQ^{\text{migration mode}} \gg Q^{\text{stationary mode}}$.

The presented motion model can also be described with a conditional density for the state transition

$$\bar{p}(x_{k+1}|x_k) \tag{10}$$

where the state is encoded as $x_k = [X_k, Y_k, \dot{X}_k, \dot{Y}_k, \delta_k]^T$

Another prior information of the kinematics of a bird is its maximum speed. However, the presented motion model does not put any restrictions on the maximum speed of the bird. On the contrary, for the constant velocity model the speed would diverge in a long time simulation. In order to include this prior information, the conditional density for state transition (10) can be slightly modified by giving it a limited support for the speed

$$p(x_{k+1}|x_k) \propto \mathbf{1}_{\|v_{k+1}\|<v_{\max}}(x_{k+1}) \cdot \bar{p}(x_{k+1}|x_k) \tag{11}$$

where $\mathbf{1}_A(x)$ is the indicator function defined as

$$\mathbf{1}_A(x) = \begin{cases} 1 & \text{if} \quad x \in A \\ 0 & \text{if} \quad x \notin A \end{cases} \tag{12}$$

and $v_k = (\dot{X}_k, \dot{Y}_k)^T$. With this modification the probability will be zero for any transition that corresponds to a speed higher than $v_{\max}$. This is in particular useful at the spring and fall equinoxes since at these occasions the sensor model (6) will be singular in latitude direction.

III. State estimation

The nonlinear filtering problem (1) will here be solved using a marginalized particle filter. For this application this is a sound approach due to many reasons:

- Like any filter, it can handle partial information of the position, so it can process sunrises and sunsets separately.
- Also like any filter, it can handle multiple modes by running two or more filters in parallel, and fusing their states according to their performance.
- The particle filter can handle multi-modal position distributions better than any other filter, which is useful for robust filtering where a lot of outliers in data occur (false and missed detections from the logged light data).
- It can handle position dependent noise, like ground vegetation type and local weather dependent noise distributions.
- It can easily include state constraints, such as maximum speed.

The time update of the position in the particle filter consists here of the following steps:

1) Simulate N noise vectors $w_k^{(i)} \sim \mathcal{N}(0, Q^{\delta_k})$.
2) Propagate the set of particles according to (8b) or (9b) depending on δ_k

If $\delta_k =$"stationary mode", the velocity is not needed in the time update. Consequently, we do not need to update the velocity. For $\delta_k =$"migration mode" we do need the velocity. However, we will see that the computation load will increase marginally.

We will here make use of the fact that the sensor model (6) depends on the position and the time only,

$$y_k = h(t_k, X_k, Y_k) + e_k. \tag{13}$$

Since the motion model is linear in the state and noise, the marginalized PF applies, so the velocity component can be handled in a numerically very efficient way.

Let $p_k = (X_k, Y_k)^T$ and $v_k = (\dot{X}_k, \dot{Y}_k)^T$. Then, (9b) and (13) can be rewritten as

$$p_{k+1} = p_k + Tv_k + \frac{T^2}{2} w_k, \tag{14a}$$
$$y_k = h(t_k, p_k) + e_k, \tag{14b}$$
$$v_{k+1} = v_k + Tw_k, \tag{14c}$$
$$p_{k+1} - p_k = Tv_k + \frac{T^2}{2} w_k. \tag{14d}$$

We here use the particle filter for (14ab) and the Kalman filter for (14cd). Note that (14ad) are the same two equations, interpreted in two different ways. The time update in the particle filter becomes

$$v_k^{(i)} = \mathcal{N}\big(\hat{v}_{k|k-1}^{(i)}, P_{k|k-1}\big), \tag{15a}$$
$$w_k^{(i)} = \mathcal{N}\big(0, Q_k\big), \tag{15b}$$
$$p_{k+1}^{(i)} = p_k^{(i)} + Tv_k^{(i)} + \frac{T^2}{2} w_k^{(i)}, \tag{15c}$$

where we treat the velocity as a noise term. Conversely, we use the position as a measurement in the Kalman filter. For this particular structure, the general result given in Theorem

2.1 in [10] simplifies a lot, and we get a combined update

$$\hat{v}^{(i)}_{k+1|k} = \frac{p^{(i)}_{k+1} - p^{(i)}_k}{T}, \tag{15d}$$

$$P_{k+1|k} = P_{k|k-1} - P_{k|k-1}\big(P_{k|k-1} + \frac{T^2}{4}Q_k\big)^{-1}P_{k|k-1}. \tag{15e}$$

Note that each particle has an individual velocity estimate $\hat{v}^{(i)}_{k|k-1}$ but a common covariance $P_{k|k-1}$. Further, for a time-invariant $Q_k = Q$, the covariance matrix converges quite quickly to $P_{k|k-1} = 0$, and the Kalman filter is in fact not needed and can be replaced with a deterministic update of the velocity.

In Algorithm 1, the update of the velocity is made in step 4c). Note that we update the velocity if the particle is in $\delta_k =$"stationary mode" as well even though it is not needed for the position update. However, that will give us an estimate of the velocity at each time instant. Furthermore, if $\delta_k =$"stationary mode" and $\delta_{k+1} =$migration mode" the velocity will be distributed with the proposal density $p_{v_0}(v)$ in order to give the particles a higher velocity more suited for the migration mode.

Finally, the particle filter gives us a straight forward way how to handle the limited support of the state transition density (11) by simply setting all weights corresponding to a speed higher than $v_{\max}$ to zero. This can be seen as using the non-saturated transition density (10) as the proposal distribution $q(x_{k+1}|x^i_k) = \bar{p}(x_{k+1}|x^i_k)$. With this interpretation, step 4a-c) in Algorithm 1 would correspond to the generation of predictions

$$x^i_{k+1} = q(x_{k+1}|x^i_k) \tag{16}$$

and the last step 4d) will compensate for the importance weights according to

$$w^i_{k+1|k} = \omega^i_{k|k}\frac{p(x_{k+1}|x^i_k)}{q(x_{k+1}|x^i_k)}. \tag{17}$$

IV. Results from Real World Data

The proposed tracking framework has been validated on real world data. This section presents this data as well as the tracking results.

A. The data

A light logger was mounted on a swift which was released from the very south of Sweden. Ten months later it was captured again at its own nest when the light logger were removed from the bird. The recorded data consists of light intensity measurements during a period of 298 days from 5th of August 2010 to 29th of May 2011. From this data the universal time of sunrise and sunset has been extracted by thresholding the data. See [11] for further details on how this has been done. The preprocessed data thus consists of the universal time of 298 sunrises and 298 sunsets as depicted in Figure 5.

Algorithm 1 Migrating bird tracking using particle filter

Choose number of particles N.

Initialization: Generate $p^i_1 \sim p_{p_0}$, $v^i_1 \sim p_{v_0}$ and $\delta^i_1 \sim p_{\delta_0}$, $i = 1, \cdots, N$, encode the state as $x^i_1 = [p^i_1, v^i_1, \delta^i_1]$ and let $\omega_{1|0} = 1/N$

Iteration over the days:

For $n = 1, 2 \cdots$

Iteration over sunrise and sunset:

For $m = \{"sunrise", "sunset"\}$

1) *Measurement update:*
For $i = 1 : N$
$$\omega^i_{k|k} = \frac{\omega^i_{k|k-1}p^m(y^m(t_k)|x^i_k)}{\sum_{j=1}^N \omega^j_{k|k-1}p^m(y^m(t_k)|x^i_k)} \tag{18}$$
2) *Estimation:* The state and covariance is estimated by
$$\hat{x}_k = \sum_{i=1}^N \omega^i_{k|k}x^i_k \tag{19}$$
$$\hat{P}_k = \sum_{i=1}^N \omega^i_{k|k}(x^i_k - \hat{x}_k)(x^i_k - \hat{x}_k)^T \tag{20}$$
3) *Resample:* Take N samples with replacement from the set $\{x^i_k\}_{i=1}^N$ where the probability to take sample i is $\omega^i_{k|k}$ and let $\omega^i_{k|k} = 1/N$
4) *Time update:*
For $i = 1 : N$
For each part of the state vector $x^i_k = [p^i_k, v^i_k, \delta^i_k]$ do the following:
a) Generate predictions of the position depending on the mode
$w^i_k \sim \mathcal{N}(0, Q^{\delta^i_k})$
If $\delta^i_k =$"stationary mode"
$p^i_{k+1} = p^i_k + Tw^i_k$
elseif $\delta^i_k =$"migration mode"
$p^i_{k+1} = p^i_k + Tv^i_k + \frac{T^2}{2}w^i_k$
b) Generate predictions of the mode
$\delta^i_{k+1} \sim p(\delta_{k+1}|\delta^i_k)$
c) Generate predictions of the velocity
If $\delta^i_{k+1} =$"mig. mode" and $\delta^i_k =$"stat. mode"
$v^i_{k+1} \sim p_{v_0}(v_0)$
else
$v^i_{k+1} = \frac{p^i_{k+1} - p^i_k}{T}$
d) Exclude particles with higher speed than $v_{\max}$
$$w^i_{k+1|k} = \frac{\omega^i_{k|k}\mathbf{1}_{\|v_{k+1}\|<v_{\max}}(x_{k+1})}{\sum_{j=1}^N \omega^j_{k|k}\mathbf{1}_{\|v_{k+1}\|<v_{\max}}(x_{k+1})}$$
5) Set $k := k + 1$

From this information the daylength and midday can easily be extracted as presented in Figure 6. The state of the art

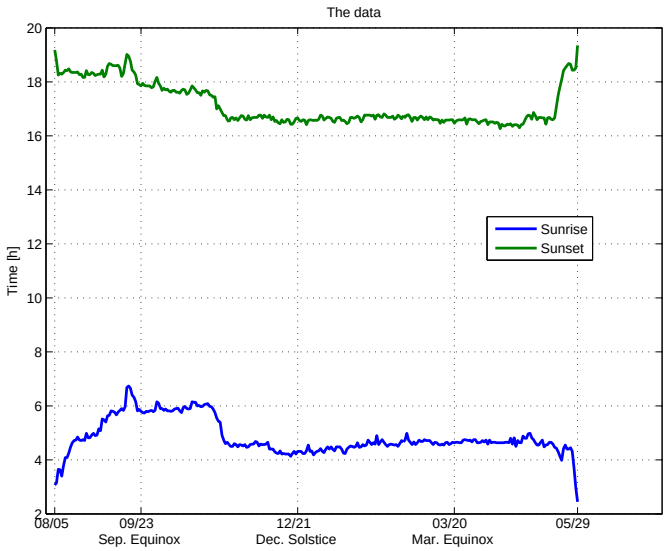

Fig. 5: Universal time of the sunrise and the sunset during the 10 moths journey of the Swift

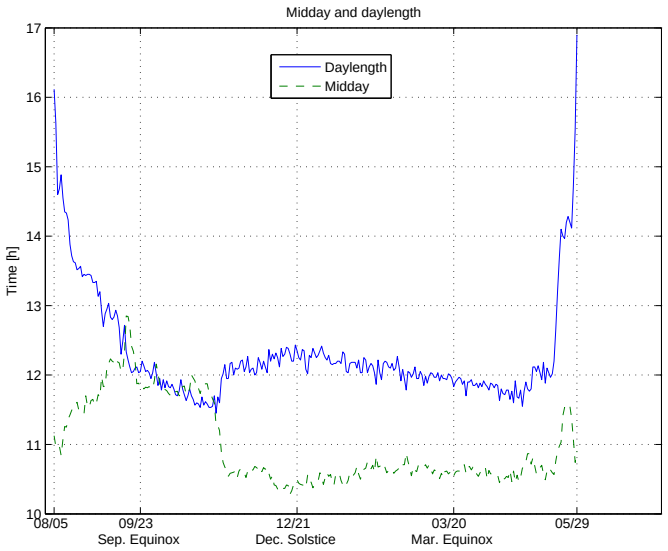

Fig. 6: The daylength and the time of the midday during the 10 months journey of the Swift.

algorithm is to use this information to convert to longitude and latitude using (2) and (5). However, with Algorithm 1 we propose to use time of sunrise and sunset to prevent the bias that would occur in fast day transitions.

Furthermore, the daylength at the equinoxes give us important information about the data. An equinox occurs when the declination of the sun (4) is equal to zero. Using (5), this gives the simplified relation

$$h^{\text{daylength}}(Y_k) = \frac{24}{360^\circ} \arccos\left(\frac{\sin h_0}{\cos Y_k}\right) \tag{21}$$

Thus, by assuming an altitude of $h_0 = 0$ for sunrise and sunset, the daylength would be 12 hours all over the world. Further, since $\cos Y_k > 0$, the sign of h_0 will decide whether the daylength is longer or shorter than 12 hours. However, by consulting the data in Figure 6 it can be noticed that the daylength is slightly longer than 12 hours at the September equinox and slightly shorter than 12 hours at the March equinox, which would require a positive h_0 and a negative h_0 respectively. As a compromise, we have here chosen $h_0 = 0$.

From the data in Figure 5 the variance of the measurement noise can be estimated. During the period from the 10th of December to the 25th of April the data is fairly constant. (As we later will see in Figure 8 this corresponds to when the Swift is at its wintering site in Africa.) This data has been detrended and is visualized as a histograms in Figure 7 for sunrise and sunset, respectively. From this data the standard deviation of the measurement noise can be estimated to approximately 5 minutes for both sunrise and sunset.

B. Results

Algorithm 1 using $N = 500$ particles has been implemented and evaluated on the presented data using the following tuning

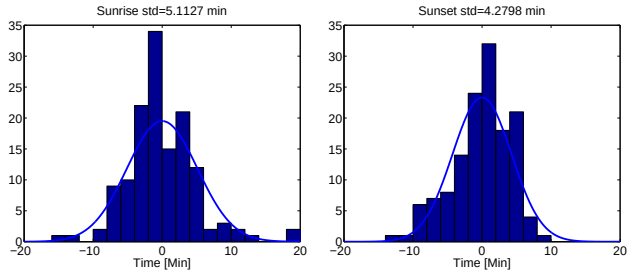

(a) Sunrise (b) Sunset

Fig. 7: Histograms for the detrended sunrise and sunset measurements from the 10th of December to the 25th of April together with a Gaussian approximation.

for the dynamics of the Swift

$$p(\delta_{k+1} = \text{"stat. mode"} | \delta_k = \text{"mig. mode"}) = 0.1 \tag{22a}$$
$$p(\delta_{k+1} = \text{"mig. mode"} | \delta_k = \text{"stat. mode"}) = 0.03 \tag{22b}$$

and

$$Q^{\delta_k = \text{"stat. mode"}} = 1^2 \cdot I_2 \tag{23a}$$
$$Q^{\delta_k = \text{"mig. mode"}} = 10^2 \cdot I_2 \tag{23b}$$

Furthermore, for the maximum speed the value $v_{\max} = 12\ [^\circ/\text{Day}] = 60$ [km/h] has been used.

The tracking performance is presented in Figure 8. The tracking result will also be compared with a non-filtering solution where we assume that the bird has not moved during the period from sunset to sunrise. Then, by using (6) and assuming $(X_k, Y_k) = (X_l, Y_l)$ the longitude and latitude can be solved uniquely each day separately. By using inverse

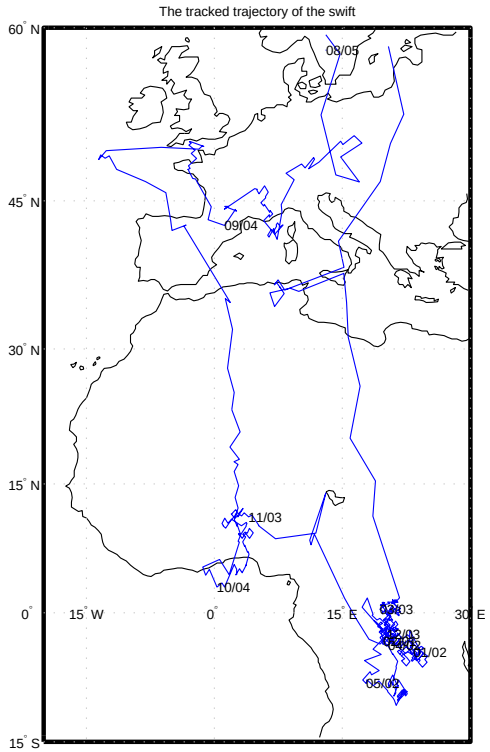

Fig. 8: The trajectory of the Swift during a period of 298 days. The positions are estimated at each sunrise and sunset.

mapping we also get a corresponding covariance

$$x_k = h^{-1}(y_k)$$
$$\mathrm{Cov}(x_k) = \left(\nabla h^T(x_k) R^{-1} \nabla h(x_k)\right)^{-1}$$

where

$$h = \begin{pmatrix} h^{\text{sunrise}} \\ h^{\text{sunset}} \end{pmatrix}, \quad y_k = \begin{pmatrix} y^{\text{sunrise}}(t_k) \\ y^{\text{sunset}}(t_k) \end{pmatrix}, \quad \text{and} \quad x_k = \begin{pmatrix} X_k \\ Y_k \end{pmatrix}.$$

In Figure 9 the estimated position for the two methods is presented together with the estimated migration mode from the particle filter implementation. Further, the estimated position is presented with a 90% confidence interval.

In Figure 10 two periods are zoomed in order to point out the differences between the two methods. According to Figure 10a, the particle filter implementation manages to mitigate the singularity due to the September equinox. The variance is still increasing for the particle filter implementation, however not as much as for the inverse mapping method. This is mainly due to the fact that we use a motion model.

As explained earlier, fast transitions in east-west direction will give rise to shorter/longer measured daylength. This will lead to a bias in the latitude estimation using the inverse mapping method since it wrongly assumes that the light logger measures the sunrise and sunset at the same position. In Figure 10b such a bias for the latitude can be seen during a period around May where the swift is making a fast transition from Africa back to Europe. The movement in west direction will

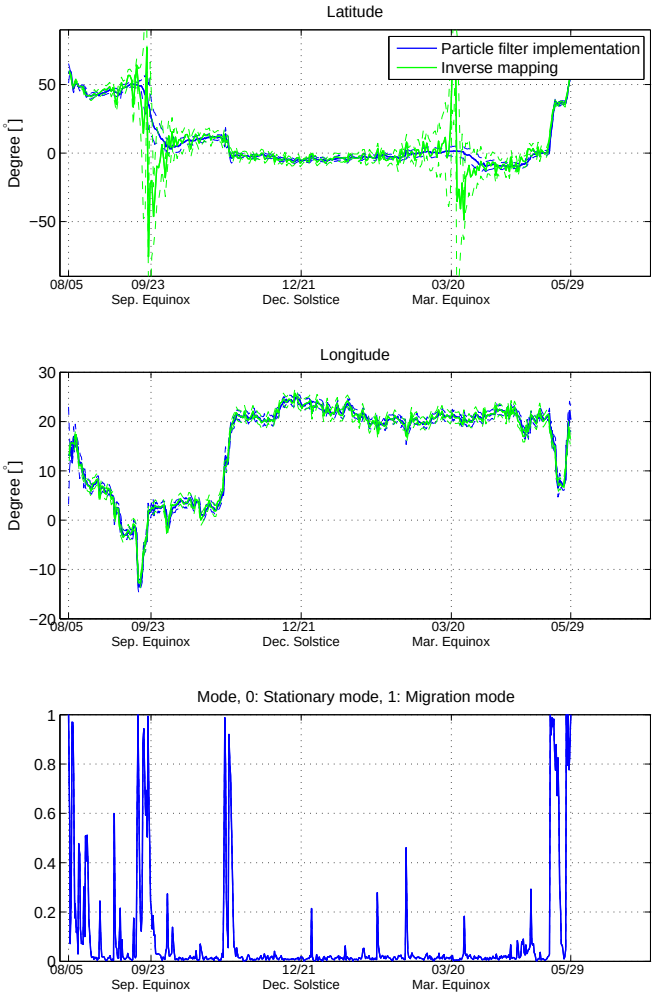

Fig. 9: The estimated position and mode of the Swift during a period of 298 days. The presented particle filter implementation is here compared with using inverse mapping. The estimates are presented with a 90% confidence interval.

make the measured daylength longer than the actual daylength at the corresponding latitude. For the inverse mapping method this will give a bias towards north since the daylength is longer on the northern hemisphere during the summer.

Finally in Figure 11 the trajectories for the particle filter implementation is presented together with covariance ellipses representing the estimation uncertainty. Here also the position of the start and end point of the journey is depicted.

V. Conclusion

In this paper, a particle filter solution has been presented estimating the trajectory of a migrating bird using light logger data. A sensor model has been presented based on astronomical formulas consisting of a measurement update at sunrise and sunset respectively, as well as a suitable motion describing the flying pattern of migrating birds. The implementation has been validated on real data and compared with the state of

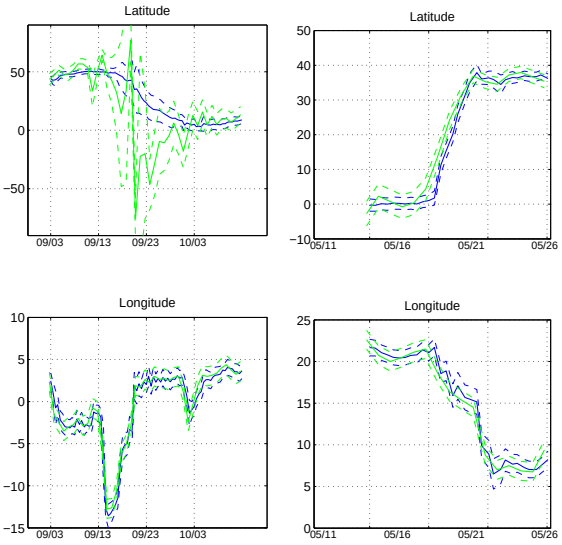

(a) September equinox (b) In the middle of May.

Fig. 10: The estimated position of the swift during a month around the fall equinox when the swift is migrating from Europe to the east of Africa as well as two weeks in the middle of May. The presented particle filter implementation (blue) is here compared with using inverse mapping (green). The estimates are presented with a 90% confidence interval.

the art algorithm based on inverse mapping. The proposed solution outperforms the existing method in reliability during the equinoxes and removes problem with bias due to fast day transitions. In addition, the proposed method provides an estimate of the migration mode suitable for further analysis of the flying pattern of the bird.

REFERENCES

[1] R. Hill, "Theory of geolocation by light levels," in *Elephant seals: population ecology, behavior, and physiology. University of California Press, Berkeley*. University of California Press.

[2] B. Stutchbury, S. Tarof, T. Done, E. Gow, P. Kramer, J. Tautin, J. Fox, and V. Afanasyev, "Tracking long-distance songbird migration by using geolocators," *Science*, vol. 323, no. 5916, p. 896, 2009.

[3] S. Åkesson, R. Klaassen, J. Holmgren, J. W. Fox, and A. Hedenström, "Migration route and strategies in a highly aerial migrant, the common swift *Apus apus*, revealed by light-level geolocators." *Submitted*.

[4] P. Smith and D. Goodman, "Determining fish movements from an archival tag: Precision of geographical positions made from a time series of swimming temperature and depth," US National Oceanic and Atmospheric Administration, Tech. Rep., 1986.

[5] R. Wilson, J. Ducamp, W. Rees, B. Culik, and K. Niekamp, "Estimation of location: global coverage using light intensity," *Wildlife telemetry: Remote monitoring and tracking of animals*, pp. 131–134, 1992.

[6] P. Ekstrom, "An advance in geolocation by light," *Memoirs of the National Institute of Polar Research*, vol. 58, pp. 210–226, 2004.

[7] J. Meeus, *Astronomical algorithms*. Willmann-Bell, Incorporated, 1991.

[8] O. Montenbruck and T. Pfleger, *Astronomy on the personal computer*. Springer Verlag, 1991, vol. 1.

[9] I. Newton, *The migration ecology of birds*. Academic Pr, 2008.

[10] T. Schön, F. Gustafsson, and P.-J. Nordlund, "Marginalized particle filters for mixed linear/nonlinear state-space models," *IEEE Transactions on Signal Processing*, vol. 53, no. 7, pp. 2279–2289, Jul. 2005.

[11] J. Fox, "Geolocator manual," 2010.

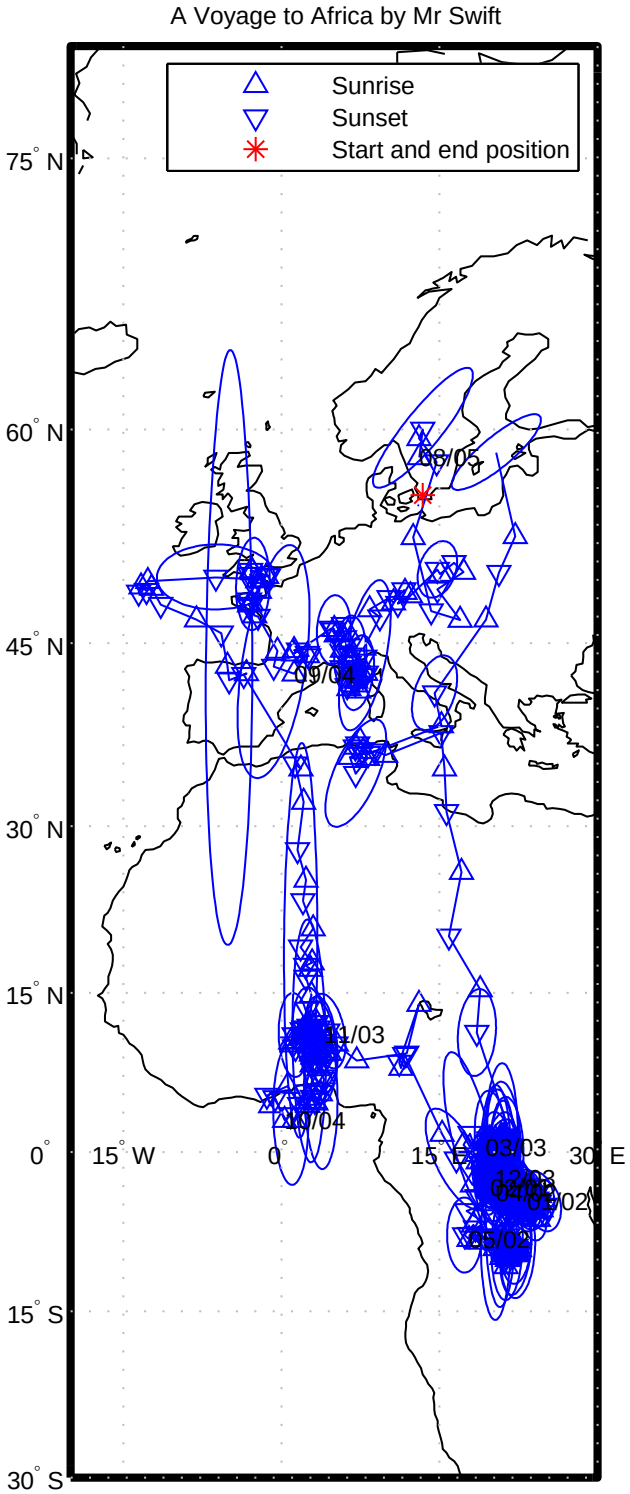

Fig. 11: The trajectory of the swift during a period of 298 days. The positions are estimated at each sunrise and sunset. At every 5th day, the accuracy of position estimate is visualized together with a 90% confidence interval.